This is the peer-reviewed, final accepted version for American Mineralogist, published by the Mineralogical Society of America.
The published version is subject to change. Cite as Authors (Year) Title. American Mineralogist, in press.
DOI: https://doi.org/10.2138/am-2022-8387. http://www.minsocam.org/

Revision 1 Word Count: 6883

Experimental determination of quartz solubility in H_2O-$CaCl_2$ solutions at 600-900 °C and 0.6-1.4 GPa

Adam R. Makhluf, Robert C. Newton, Craig E. Manning

Department of Earth, Planetary and Space Sciences
University of California, Los Angeles
Los Angeles, CA, USA 90095-1567

Corresponding author:
Craig Manning
manning@epss.ucla.edu
(310) 206-3290

Abstract

Fluid-mediated calcium metasomatism is often associated with strong silica mobility and the presence of chlorides in solution. To help quantify mass transfer at lower crustal and upper mantle conditions, we measured quartz solubility in H_2O-$CaCl_2$ solutions at 0.6-1.4 GPa, 600-900 °C, and salt concentrations to 50 mol%. Solubility was determined by weight loss of single-crystals using hydrothermal piston-cylinder methods. All experiments were conducted at salinity lower than salt saturation. Quartz solubility declines exponentially with added $CaCl_2$ at all conditions investigated, with no significant evidence for complexing between silica and Ca. The decline in solubility is similar to that in H_2O-CO_2 but substantially greater than that in H_2O-NaCl at the same pressure and temperature. At each temperature, quartz solubility at low salinity ($X_{CaCl2} < 0.1$) depends strongly on pressure, whereas at higher X_{CaCl2} it is nearly pressure independent. This behavior is consistent with a transition from an aqueous solvent to a molten salt near $X_{CaCl2} \sim 0.1$. The solubility data were used to develop a thermodynamic model of H_2O-$CaCl_2$ fluids. Assuming an ideal molten salt behavior and utilizing previous models for

polymerization of hydrous silica, we derived values for the activity of H_2O (a_{H2O}), and for the $CaCl_2$ dissociation factor (α), which may vary from 0 (fully associated) to 2 (fully dissociated). The model accurately reproduces our data along with those of previous work and implies that, at conditions of this study, $CaCl_2$ is largely associated (<0.2) at H_2O density <0.85 g/cm^3. Dissociation rises isothermally with increasing density, reaching ~1.4 at 600 °C, 1.4 GPa. The variation in silica molality with a_{H2O} in H_2O-$CaCl_2$ is nearly identical to that in H_2O-CO_2 solutions at 800 °C and 1.0 GPa, consistent with the absence of Ca-silicate complexing. The results suggest that the ionization state of the salt solution is an important determinant of a_{H2O}, and that H_2O-$CaCl_2$ fluids exhibit nearly ideal molecular mixing over a wider range of conditions than implied by previous modeling. The new data help interpret natural examples of large-scale Ca-metasomatism in a wide range of lower crustal and upper mantle settings.

Key words: metasomatism, quartz, silica, experimental, brines, fluids, halogens, solubility

1. Introduction

Fluid-mediated replacement of rock bodies with calcium silicate and/or carbonate assemblages (Ca-metasomatism) is an important process in the earth's crust and upper mantle. Ca-metasomatized metamorphic rocks are found in various lithologies and grades, from surficial to deep-crustal and upper mantle parageneses. Examples include "epidosites" and prehnite-pumpellyite rocks after intermediate and mafic lithologies (Harper, 1995), lawsonite-replaced blueschists and eclogites (Brovarone and Beyssac, 2014), rodingite alteration of ultramafic rocks (Python et al., 2011), scapolite-rich rocks after granites, metasediments and sodic anorthosites (Oliver et al., 1994, Moecher et al., 1992), and fluid-induced formation of calcic clinopyroxene in low-Ca diamondiferous peridotites (Schulze, 1995). Carbonated "megashear" terranes such as the Late Precambrian Attur Valley of southern India (Wickham et al., 1994) show replacement of up to 20% of the dominantly quartzofeldspathic country rocks by calcite or dolomite. Of considerable interest to economic geology is the conspicuous involvement of Ca-metasomatism in the genesis of major Au, Cu and rare-earth element deposits, as in the Cloncurry District of Queensland, Australia (Mark et al., 2006), the Zambian "Copperbelt" (Eglinger et al., 2014) and the porphyry Cu ore body at Yerington, Nevada (Carten, 1986). The presence of Ca^{2+} ions in ore-forming fluids can facilitate disproportionation of an SO_2-bearing fluid to form anhydrite and sulfides (Mavrogenes and Blundy, 2017).

Mobilization and transport of Ca is facilitated by chloride in aqueous solutions, as shown by fluid inclusion studies of metasomatized rocks (De Jong and Williams, 1995). These fluids promote high mobility of alkalis and alkaline earths in exchange processes involving feldspar, and pervasive replacement, consonant with the high "wetting" ability of chloride solutions (Holness, 1992). However, little is known about the actual nature of the solutions: their

concentrations, acid-base relations, accompanying cations and anions such as carbonate and sulfate, specific interaction with mineral assemblages, or mode of origin, whether magmatic (Mark, 1998), diagenetic (Kendrick et al., 2008) or evaporitic (Oliver et al., 1994).

Ca metasomatism is commonly associated with substantial silica mobility. The combination of Ca and Si mobility with chloride-bearing fluids motivates examination of the nature of silica dissolution in the presence of Ca and Cl in solution. Measurements of the solubility of quartz in $CaCl_2$ solutions at high pressure (P) and temperature (T) are an important starting point. Shmulovich et al. (2006) measured quartz solubility in H_2O-$CaCl_2$ fluids over a wide range of temperature (400-800 °C), pressure (0.1-0.9 GPa) and salt concentration (50-100 mol% H_2O). They found that $CaCl_2$ causes strong decrease of quartz solubility at all P >0.2 GPa. The decrease in solubility is stronger than they observed in H_2O-NaCl fluids at the same P, T, and salt concentration. Quartz solubility in H_2O-NaCl exhibits initial increase at low NaCl ("salting in") at P up to ~0.5 GPa (Novgorodov, 1975; Novgorodov, 1977; Xie and Walther, 1993; Newton and Manning, 2000; Shmulovich et al., 2006). At higher P, solubility declines monotonically with NaCl concentration but the decrease is subdued relative to that seen in solutions with inert diluents such as CO_2 (e.g., Newton and Manning, 2000, 2009; Shmulovich et al., 2001, 2006). Shmulovich et al. (2006) showed that other alkali chlorides exhibit similar trends. Explanations for this behavior include density effects in the solvent (e.g., Fournier, 1983; Akinfiev and Diamond, 2009; Brooks and Steele-MacInnis, 2020) and complexing between silica and salt components (e.g., Evans, 2007; Newton and Manning, 2010, 2016).

The difference in quartz solubility behavior in aqueous solutions of $CaCl_2$ vs alkali halides revealed by the data of Shmulovich et al. (2006) has not been explained. Shmulovich et al. (2006) empirically fit their measurements at each P and T, but did not attempt a more

comprehensive model. Potential effects of silica speciation and complexing, and mixing properties of the fluid phase were not considered. To address these issues, we investigated the solubility of quartz in H_2O-$CaCl_2$ solutions at 0.6, 1.0 and 1.4 GPa from 600-900 °C. Our new data provide a framework for modeling silica dissolution in this geologically important fluid. The new results allow quantification of silica transport in Ca-metasomatic environments in a range of deep crustal and upper mantle settings.

2. Experimental methods

2.1 Starting materials and sample loading

Experimental methods generally followed those of Manning (1994) and Newton and Manning (2000), in which the weight loss of single crystals was used to measure solubility. Starting materials consisted of high purity quartz from Brazil (Manning, 1994), 18 MΩ-cm deionized water, and EMD brand anhydrous $CaCl_2$. Fragments of 1-3 mm long quartz were initially rounded with a diamond file to remove sharp edges, then further rounded with 600 and then 400 grit sandpaper. The crystals were sonicated in ethanol or acetone to remove adhering debris and then heated in a 600 °C oven to purge organic residue. Starting crystal weights were ~0.5-14.0 mg. Unfractured run-product crystals were reused in successive experiments.

The experiments employed Pt capsules fabricated from tubing (3.5 mm OD, 0.25 mm wall thickness). After cleaning with acetone, the bottom of a ~1.6 cm long piece of tubing was crimped and welded using a graphite arc-welder. A quartz crystal was first loaded into the tubing, followed by $CaCl_2$. To minimize H_2O absorption during loading of hydroscopic $CaCl_2$, the salt was stored in an oven at 600 °C, then loaded and weighed within 1-2 min of removal from the oven. Deionized water (10-40 mg) was then added with a microliter syringe. The top of

the capsule was crimped with pliers and sealed by arc welding. Average weight loss upon sealing was 0.4 mg, all of which results from Pt evaporation based on numerous sealing tests on dry and H_2O-filled capsules. All weights were measured with a Mettler-Toledo UXM2 ultra micro balance with an uncertainty of 0.2 μg.

2.2 Piston-cylinder Methods

Experiments were conducted in a 2.54 cm piston-cylinder apparatus at 0.6-1.4 GPa and 600-900 °C. Pressure was measured with a Heise bourdon tube gauge, and temperature was controlled on a Eurothem 2208e controller using type-S ($Pt-Pt_{90}Rh_{10}$) thermocouples. Pressure and temperature uncertainties are estimated to be ±0.03 GPa and ±3 °C, respectively. No correction was made for the effect of pressure on thermocouple emf.

The furnace assembly was similar to that in Fig. 1A of Johannes et al. (1971), but with NaCl or NaCl/BN pressure media. An NaCl pressure medium was used in experiments at 600-800 °C. No pressure correction was applied (Johannes, 1973; Mirwald et al., 1975). For experiments at 900 °C, an NaCl pressure medium was used in combination with 0.38 cm BN inserts placed above and below the sample to improve mechanical stability near the NaCl melting point. The BN-NaCl pressure medium required a pressure correction of -60 MPa relative to the NaCl pressure medium, determined by comparison with quartz solubility in H_2O measured in NaCl-only pressure media (Manning, 1994). The samples were heated resistively using cylindrical graphite heater sleeves of 3.18 cm in length, 1.50 cm outer diameter and 0.165 cm wall thickness.

The capsule was loaded horizontally at the midpoint of the graphite furnace on either a 1.27 cm cylinder of compressed NaCl or on a 0.38 cm cylindrical piece of compressed BN on

top of a 0.89 cm cylinder of compressed NaCl. The capsule was embedded in either NaCl or BN powder. A platinum disc of ~0.64 mm thickness was placed in contact with the capsule in order to prevent puncturing by the tip of the thermocouple. Slight indentation on quenched capsules proved thermocouple contact.

The cold piston-in technique was used for all experiments. P-T paths varied because of the relatively large range of P-T conditions investigated. For experiments at 600 °C and 0.6 GPa, the samples were pressurized to a nominal 0.3-0.5 GPa and then heated to 600 °C. Further pressurization was required to reach the target value. At 700-800 °C and 0.6 GPa the samples were pressurized to 0.35 GPa, followed by increasing the temperature to the target value. At these conditions, the temperature was high enough that the target pressure was reached or only minimal further pressurization was required. For experiments conducted at 1.0 GPa, the samples were cold pressed to ~30% below the target pressure and then heated to the final temperature. Gauge pressure rose to the final target value and was bled in order to maintain the desired pressure. For runs at 1.4 GPa, the samples were pressurized to 0.75 GPa, heated to 100 °C, and then further pressurized to 1.2 GPa. The samples were then heated to their target value where upon the pressure rose and was bled to maintain the final pressure. Run times for the experiments were typically about 20 hrs. Runs were quenched by turning off the power, dropping the temperature to < 200°C in ~30 seconds.

2.3 Solubility determination

After each experiment, platinum capsules were cut open with a razor, placed in an agate mortar and irrigated with water to remove the contents of the capsules. All crystals were carefully inspected using a binocular microscope. The quartz crystals were unbroken after most

runs. Unbroken quartz crystals were sonicated in ethanol or water to remove adhered quench product and residual $CaCl_2$, then dried at 110 °C and weighed. For experiments in which the crystal broke, multiple irrigation steps were performed to remove all of the $CaCl_2$ from the solution. A platinum weighing boat of known mass was then immersed in water and the crystals transferred to it with pair of ultra-fine-tip tweezers. This was done under a binocular microscope to assure that all quartz fragments were collected. The platinum boat containing the crystal fragments was then dried at 110°C and weighed. In all cases, solubility was taken to be the difference in crystal weight.

3. Results

The results of 78 experiments on quartz solubility in H_2O-$CaCl_2$ fluids are presented in Table 1. Quench pH was determined in selected experiments. All were neutral to slightly acidic (5.0-7.5).

We ensured that run durations were sufficient to attain equilibrium by conducting a time series at 600 °C, 1.0 GPa, and X_{CaCl2} = 0.26. These conditions represent the lowest temperature and one of the higher salt contents investigated. Run times in four experiments varied between 1.5 and 18 hr (Table 1). The 1.5 hr run returned slightly lower solubility than the three longer runs, which gave similar results independent of time and were therefore assumed to have equilibrated. This is consistent with Newton and Manning (2000), who found equilibration times of ~2 hr for quartz dissolution in aqueous NaCl solutions at 700 °C and 1.0 GPa. Based on these considerations, all runs at 600 °C were at least 17.5 hr. Some runs at higher T had shorter run times, but none were shorter than the minimum duration of the time series.

The experimental results are presented in Fig. 1. The starting crystal was chipped or broken in ten runs (13% of experiments). In all cases, the pieces could be recovered and weighed; however, the chance that a few stray fragments were missed means that these runs strictly provide only a maximum constraint on solubility. In run QzC-56, several minute euhedral quartz crystals were interpreted to have grown during the run though the crystal showed no evidence of mechanical failure. In this case, the crystals were collected and their mass included with the final quartz weight in determining solubility. As with runs in which the crystal broke, this experiment is taken as a maximum solubility constraint. Figure 1 shows that maximum-solubility results agree well with the rest of the data at any given P and T. Nevertheless, these data were omitted from all fitting and modeling described below.

Table 1 includes new data on quartz solubility in pure H_2O. These data are in good agreement with previous predictions (Manning, 1994; Dolejš and Manning, 2010; Hunt and Manning, 2012; Sverjensky et al., 2014). Our new pure-H_2O data are used to establish the trends in Fig. 1 and in modeling; however, where we did not conduct new experiments in pure H_2O, we used the solubility equation of Hunt and Manning (2012) in preference to those of Manning (1994), Dolejš and Manning (2010) or the DEW model (Sverjensky et al., 2014) because it provides the best agreement with experimental results at 900°C while yielding accuracy similar to the other models at lower temperature.

The results show that, at all of the investigated P and T, quartz solubility is highest in pure H_2O but declines exponentially with increasing mole fraction of $CaCl_2$, as indicated by the isobaric-isothermal linear trends in Fig. 1a-c. Fitted linear slopes are broadly independent of pressure and become less negative with rising temperature. No evidence for salt saturation was observed.

This is the peer-reviewed, final accepted version for American Mineralogist, published by the Mineralogical Society of America.
The published version is subject to change. Cite as Authors (Year) Title. American Mineralogist, in press.
DOI: https://doi.org/10.2138/am-2022-8387. http://www.minsocam.org/

At some conditions, quartz solubility in NaCl-H_2O fluids increases slightly before declining at low NaCl concentrations (Xie and Walther, 1993; Newton and Manning, 2000; Shmulovich et al., 2006). This effect was not observed here, except possibly at the lowest pressure of 0.6 GPa and 800 °C (Fig. 1a). At any given temperature, quartz solubility is nearly independent of pressure for $CaCl_2$ mole fraction (X_{CaCl_2}) more than ~0.1 (Fig. 1d). This behavior is similar to quartz solubility in concentrated NaCl solutions and is consistent with a transition from an aqueous solution dominated by the effects of solvent H_2O, to a solution which behaves more like a molten salt dominated by the $CaCl_2$ component (Newton and Manning, 2000).

4. Discussion

4.1 Thermodynamic model

A thermodynamic framework for explaining quartz solubility in $CaCl_2$ solutions can be developed by comparison to quartz solubility behavior in H_2O-NaCl and H_2O-CO_2. Figure 2a shows the change in quartz solubility at 800 °C and 1 GPa as NaCl (Newton and Manning, 2000), CO_2 (Newton and Manning 2000, 2009), or $CaCl_2$ (this study) are added to H_2O. In each case, the solubility declines as the concentration of the added component increases. Notably, the extent of the decline differs depending on the component, with the decline associated with adding $CaCl_2$ slightly greater than for the same molar amount of CO_2, and significantly greater for NaCl. Various models have been developed to explain such differences at high P and T. Largely empirical approaches based on solvent density have been successful for H_2O-CO_2 and/or H_2O-NaCl (e.g., Shmulovich et al, 2006; Akinfiev and Diamond, 2009; Brooks and Steele MacInnis, 2020). An alternative framework is based on solvent mixing models and solute-solvent interaction (e.g., Newton and Manning, 2009, 2010, 2016). However, both approaches

pose problems for the present data set because of uncertainty in the properties and behavior of H_2O-$CaCl_2$ solutions at high P and T. Ivanov and Bushmin (2019) have proposed a model for H_2O-CO_2-$CaCl_2$ fluids at conditions relevant to this study. Their model reproduces ternary phase-equilibrium experiments; however, its accuracy for H_2O activity and $CaCl_2$ speciation on the H_2O-$CaCl_2$ binary is unknown. Here we use our new quartz solubility data to simultaneously develop a provisional model for quartz solubility and H_2O activity in H_2O-$CaCl_2$ solutions at high P and T.

Development of the model begins by consideration of the nature of dissolved silica. In the absence of strong shifts from neutral pH, dissolved silica exists as neutral species in varying states of polymerization (Zhang and Frantz, 2000; Zotov and Kepler, 2000, 2002; Newton and Manning, 2002, 2003). For most deep crustal conditions, the monomer and the dimer predominate in pure H_2O (Newton and Manning, 2008; Huang and Sverjensky, 2019). Both can be modeled as hydrous species containing both structurally bound OH groups as well as molecular H_2O of solvation. Water activity in mixed fluids can therefore be expected to play an important role in the stability of silica species, and hence in quartz solubility. This is seen by considering homogeneous equilibrium between the monomer and dimer

$$2Si(OH)_4 \cdot (n-2)H_2O = Si_2O(OH)_6 \cdot (2n-1)H_2O + H_2O \quad (1)$$

in which *n* is the "hydration number" of dissolved silica (e.g., Walther and Orville, 1983; Newton and Manning, 2009) reflecting the sum of H_2O necessary to form OH groups and molecular H_2O tightly solvated to the complex. The equilibrium constant for monomer-dimer equilibrium (K_{md}) in Eq. 1 is

This is the peer-reviewed, final accepted version for American Mineralogist, published by the Mineralogical Society of America.
The published version is subject to change. Cite as Authors (Year) Title. American Mineralogist, in press.
DOI: https://doi.org/10.2138/am-2022-8387. http://www.minsocam.org/

$$K_{md} = \frac{a_d a_{H_2O}}{a_m^2} \quad (2)$$

where *a* denotes activity and *m* and *d* stand for the monomer and dimer. Newton and Manning (2002) compared solubilities of SiO_2-buffering assemblages to show that, at conditions of the present experiments, values of K_{md} are accurately represented by

$$\log K_{md} = 1.48 + 0.0012\mathrm{T} + (0.000119\mathrm{T} - 0.1685)\mathrm{P} \quad (3)$$

with T in Kelvins and P in kbar. Equation 3 yields silica speciation that is consistent with experimental solubility and spectroscopic results of Zhang and Frantz (2000), Zotov and Keppler (2000, 2002) and Newton and Manning (2002, 2003), but not with data from Sverjensky et al. (2014). Moreover, the latter source yields unrealistic results when extrapolated to low pressure, so Eq. 3 was used in preference. It is important to note that the model results described below do not depend strongly on the silica speciation model.

Equilibrium between quartz and the monomer can be written:

$$SiO_2 + nH_2O = Si(OH)_4 \cdot (n-2)H_2O \quad (4)$$

for which the equilibrium constant, K_{qm}, is

$$K_{qm} = \frac{a_m}{a_{H_2O}^n} \quad (5)$$

This is the peer-reviewed, final accepted version for American Mineralogist, published by the Mineralogical Society of America.
The published version is subject to change. Cite as Authors (Year) Title. American Mineralogist, in press.
DOI: https://doi.org/10.2138/am-2022-8387. http://www.minsocam.org/

The H_2O activity in H_2O-$CaCl_2$ fluids may then be derived from the quartz solubility measurements:

$$a_{H_2O} = \left(\frac{a_m}{K_{qm}}\right)^{1/n} \quad (6)$$

Newton and Manning (2009) found, by measurements of quartz solubility in H_2O-CO_2 solutions, that *n* is a constant equal to 4 for a wide range of P and T.

Following Newton and Manning (2002, 2003, 2009), we take the standard state for total silica in solution (a_{SiO2}) to be unit activity of the hypothetical pure solution of the monomer, and the activities of silica species to be equal to their mole fractions; i.e., they mix ideally. These conventions lead to

$$a_{SiO2} = \gamma_{SiO2} X_{SiO2} = X_m = a_m \quad (7)$$

and

$$a_d = X_d \quad (8)$$

where *X* denotes mole fraction and γ_{SiO2} is the activity coefficient for total dissolved SiO_2, which can be determined from the mole fraction of total dissolved SiO_2 (X_{SiO_2}) and Eq. 3:

$$\gamma_{SiO_2} = \frac{-1+\left(8K_{md}X_{SiO_2}^{-1}\right)^{1/2}}{4K_{md}X_{SiO_2}} \quad (9)$$

This is the peer-reviewed, final accepted version for American Mineralogist, published by the Mineralogical Society of America.
The published version is subject to change. Cite as Authors (Year) Title. American Mineralogist, in press.
DOI: https://doi.org/10.2138/am-2022-8387. http://www.minsocam.org/

Taking the standard state for H_2O to be unit activity of the pure phase and neglecting the effect of SiO_2 on H_2O, K_{qm} is determined at each P and T from the solubility of quartz in pure H_2O (Eqs. 5 and 9). This allows derivation of H_2O activity from quartz solubility measurements in H_2O-$CaCl_2$ (Eq. 6).

Our model for H_2O-$CaCl_2$ mixing follows Aranovich and Newton (1996, 1997), who showed that in H_2O-NaCl and H_2O-KCl solutions at high P and T, there is a marked decrease in a_{H2O}/X_{H2O} that occurs at P greater than about 0.3 GPa. They interpreted this to result from pressure-induced ionization of the alkali chlorides (e.g., Quist and Marshall, 1966). This led Aranovich and Newton to adopt an ideal fused-salt model for H_2O activity in salt solutions, in which

$$a_{H_2O} = X_{H_2O}/(1 + \alpha X_{salt}) \tag{10}$$

where α is the dissociation parameter which nominally varies from zero for an undissociated salt to one for a single salt such as NaCl fully dissociated to Na^+ and Cl^-. $CaCl_2$ dissociates in two steps via formation of $CaCl^+ + Cl^-$ followed by $Ca^{+2} + 2Cl^-$. Thus, for consistency with the fused salt model, we set α for $CaCl_2$ to vary from 0 to 2. The mole fraction of silica is related to the experimentally determined SiO_2 molality (m_{SiO2}, Table 1) by:

$$X_{SiO_2} = X_m + 2X_d = \frac{m_{SiO_2}}{m_{SiO_2} + 55.51\left(1 + \frac{(1+\alpha)X_{CaCl_2}}{1 - X_{CaCl_2}}\right)} \tag{11}$$

Values of α in the fused salt model are constants independent of concentration (e.g., Newton and Aranovich, 1996). In the context of this study, α can be interpreted to be an average over an experimentally investigated concentration range.

We used Eqs. 6-11 in combination with experimental results (Table 1) to derive values of α at each investigated P and T by weighted least squares regression. Figure 2c shows an example result at 800 °C, 1 GPa, where $\alpha = 0.17$ yields a best fit to the data. Solubility behavior for $\alpha = 0$, 1, and 2 is shown for reference, along with predicted solubility using $\alpha = 1.51$ calculated from the model of Ivanov and Bushmin (2019). At 800 °C and 1 GPa, the Ivanov and Bushmin model predicts that $CaCl_2$ is strongly dissociated, yielding a_{SiO_2} and m_{SiO_2} that are too low to be consistent with observed quartz solubility. The solubility data instead imply that $CaCl_2$ is only slightly dissociated at these conditions.

The modeling approach described above assumes that a_{H_2O} is the sole control on quartz solubility, which is justified because dissolved silica species are hydrated (Eq. 1). If a_{H_2O} is the only controlling factor, the array of solubility values at a constant T and P plotted against H_2O (or salt) mole fraction correspond to lines of constant alpha, as in Fig. 2b. If, however, SiO_2 complexes with the salt component, there is an additional increment of solubility or "enhancement". This leads to contrasting solubility behavior in plots of H_2O activity vs. SiO_2 concentration. For example, there is no evidence for complexing between SiO_2 and CO_2 in H_2O-CO_2 fluids (e.g., Walther and Orville, 1983; Newton and Manning, 2009), which leads to a strong decline in quartz solubility with a_{H2O} (Fig. 2c). In contrast, quartz solubility declines less strongly with a_{H_2O} in H_2O-NaCl (Fig. 2c), which can be interpreted as a consequence of Na-SiO_2 complexing (e.g., Evans, 2007; Newton and Manning, 2016) and is consistent with the extreme solubility of Na silicates. In this case, mass balance (Eq. 11) must be modified such that

This is the peer-reviewed, final accepted version for American Mineralogist, published by the Mineralogical Society of America.
The published version is subject to change. Cite as Authors (Year) Title. American Mineralogist, in press.
DOI: https://doi.org/10.2138/am-2022-8387. http://www.minsocam.org/

$$X_{SiO_2} = X_m + 2X_d + \sum_i \nu_i X_i \quad (12)$$

where *i* refers to the additional silica complexes and ν_i is the number of Si in a complex.

The low solubility of wollastonite ($CaSiO_3$) in pure H_2O at 800 °C, 1 GPa (Newton and Manning, 2006) suggests negligible of SiO_2-Ca complexing. This is confirmed by the lower solubility of quartz in $CaCl_2$-H_2O than in H_2O-CO_2 (Fig. 2a). Fig. 2c shows that the predicted variation in quartz solubility with a_{H_2O} with no SiO_2-Ca complexing is nearly identical in the H_2O-$CaCl_2$ and H_2O-CO_2 systems. The much higher solubility of quartz in NaCl solutions (Fig. 2c) of the same H_2O activity is consistent with the inferred strong Na-SiO_2 complexing in that medium.

Best-fit values of the dissociation factor, α, were found to increase with P at constant T, and to decrease with T at constant P (Table 2). These values were fitted to polynomial function of P and T, which supplied smoothed values of α for fitting to a logistic function of the form

$$\alpha = \frac{2}{1+e^{-k(\rho_{H_2O}-\rho^*_{H_2O})}} \quad (13)$$

where ρ_{H_2O} is H_2O density in g/cm^3. Equation 13 forces α to vary from zero to two, consistent with the fused salt model. Least squares regression gave optimal values of the parameters *k* and $\rho^*_{H_2O}$ as functions of P (GPa):

$$k = 75.26 - 36.94P \quad (14)$$

$$\rho^*_{H2O} = 0.665 + 0.4268P - 0.1196P^2 \quad (15)$$

This is the peer-reviewed, final accepted version for American Mineralogist, published by the Mineralogical Society of America.
The published version is subject to change. Cite as Authors (Year) Title. American Mineralogist, in press.
DOI: https://doi.org/10.2138/am-2022-8387. http://www.minsocam.org/

Values of ρ_{H2O} were from Holland and Powell (1991), and all parameters were assigned dimensions consistent with dimensionless α. In Eq. 13, ρ^*_{H2O} may be regarded as a characteristic density of the solution, and the parameter *k* determines the span and the slope of the α function. Values of α derived from Eq. 13 are given in Table 2.

Figure 3 compares solubilities from Eq. 13 with experimental results. Overall the model reproduces the data well. However, in detail the fits somewhat poorer at the highest temperatures at each pressure. This could be a consequence of some combination of the appearance of low concentrations of more polymerized silica at these conditions (Newton and Manning, 2008; Hunt and Manning, 2012), less accurate experimental results where solubilities are highest, and the slim possibility of SiO_2-Ca complexing leading to "salting in" at 0.6 GPa, 800 °C, and the lowest X_{CaCl2} (run QzC-74).

4.2 Comparison to previous results

Shmulovich et al. (2006) determined quartz solubility in H_2O-$CaCl_2$ fluids at selected conditions in the range 0.1-0.9 GPa, 400-800 °C. Figure 4 shows their results at conditions similar to those of the present study. They modeled their solubility data in a form similar to that of Setchénow (1892):

$$\log m_{SiO_2} = 3.5 \log X_{H_2O} + a * m^b_{salt} \quad (16)$$

where the *m* denotes molality. The coefficient 3.5 is similar to the hydration number *n* (Eqs. 1 and 4), but differs in detail because X_{H_2O} rather than a_{H_2O} is used. Shmulovich et al. (2006)

This is the peer-reviewed, final accepted version for American Mineralogist, published by the Mineralogical Society of America.
The published version is subject to change. Cite as Authors (Year) Title. American Mineralogist, in press.
DOI: https://doi.org/10.2138/am-2022-8387. http://www.minsocam.org/

derived empirical constants *a* and *b* which are unique to each P, T, and salt in their study, but they did not identify any systematics in their variations. Nevertheless, this empirical approach accurately represents their data, as shown in Fig. 4.

Figure 4 also illustrates quartz solubility predicted by Eq. 13. The Shmulovich et al. (2006) data are reproduced by our model with accuracy comparable to their Setchénow parameters.

Thermodynamic modeling using data from Huang and Sverjensky (2019) suggests that the aqueous calc-silicate complex, $Ca(H_3SiO_4)^+$, contributes significantly to total dissolved silica, such that predicted quartz solubility initially rises with addition of minor $CaCl_2$ at all P and T of our study. This is not seen in our results (Figs. 1 and 3), and thus the experimental data require substantially lower stability of any such calc-silicate complex. The neutral to slightly acidic quench pH of the present solutions (5-7.5) suggests that the deprotonated silica dimer ($Si_2O_4(OH)^-$), inferred by (Aranovich et al., 2020) for quartz solubility in Na_2CO_3 solutions at 0.4 GPa, is not a major species in $CaCl_2$-H_2O solutions.

4.3 Implications for H_2O-$CaCl_2$ fluids

Figure 5 illustrates the variation in α consistent with our experiments at mid- to lower-crustal and upper mantle conditions. At these conditions, our model suggests that $CaCl_2$ is largely associated ($\alpha = 0$) at ρ_{H_2O} below ~0.8. Dissociation becomes significant at higher density along any isotherm or isobar. Our results contrast with predicted α in the model of Ivanov and Bushmin (2019), in which the transition from associated to largely dissociated $CaCl_2$ occurs at much lower density, leading to near constant predicted α of 1.5±0.1 over the conditions of this study.

This is the peer-reviewed, final accepted version for American Mineralogist, published by the Mineralogical Society of America.
The published version is subject to change. Cite as Authors (Year) Title. American Mineralogist, in press.
DOI: https://doi.org/10.2138/am-2022-8387. http://www.minsocam.org/

Variations in α can be used to assess activity-composition relations in H_2O-$CaCl_2$ fluids. Figure 6 shows a_{H_2O} vs. X_{H_2O} (Eq. 10) at the conditions of our experiments. In the ideal fused salt model, $a_{H_2O} = X_{H_2O}$ where α = 0 consistent with ideal molecular mixing. Maximum negative departures of a_{H_2O} from X_{H_2O} occur where α = 2, corresponding to ideal mixing of a fully dissociated double salt. Figure 6a illustrates *a*-*X* relations at 1.0 GPa and 700 °C. At this P and T, we obtain α = 0.45, consistent with only a small negative departure from $a_{H_2O} = X_{H_2O}$; i.e., comparatively minor dissociation. The model of Ivanov and Bushmin (2019) gives α = 1.53, implying with more extensive dissociation and stronger departure from the 1:1 line. At each pressure, our results indicate progressive approach to ideal molecular mixing (increasing association, decreasing α) with rising temperature (Fig. 6b-d). Isothermal pressure increase causes α to rise, yielding progressively greater departures from the 1:1 line.

4.4 Applications to petrology

Our results on the solubility of quartz in H_2O-$CaCl_2$ fluids may be useful in modeling silica metasomatism in settings showing evidence for calcium and other chlorides in solution. For example, in the Cloncurry District of Queensland, conversion of metabasic and metapelitic lithologies to actinolite-titanite-clinopyroxene-rich rocks along with possibly metasomatic quartzites record high silica mobility, and fluid inclusions in the quartz high levels of both $CaCl_2$ and NaCl (De Jong and Williams, 1995). The observations are consistent with regional-scale scapolite alteration in the district (Edwards and Baker, 1953).

Alpine eclogites and blueschists of Corsica have undergone conversion to lawsonite-rich rocks containing as much as 13 wt. % CaO and 12 wt. % H_2O, with strong silica depletion and almost total removal of K_2O (Brovarone and Beyssac, 2014). Metasomatic scapolite is a striking

feature of the Bamble Shear Belt of southern Norway (Touret and Nijland 2013). This region also features extensive wholesale metasomatic replacement of silicate rocks by dolomite (Dahlgren et al., 1993). Depletion of silica is profound in this occurrence. At very high pressures and temperatures, i.e. upper mantle conditions, $CaCl_2$ can coexist with alkali chlorides in the dissociated state in concentrated solutions comparable to fused salt mixtures, as in fluid inclusions in cloudy diamonds (e.g., Izraeli et al., 2001). The metasomatizing potential of these fluids is, as yet, undefined, but must be substantial.

The important inference that can be drawn from these natural occurrences is that, in light of the decrease in quartz solubililty with increasing $CaCl_2$ (this study) and NaCl (Fig. 1; Newton and Manning 2000), integrated fluid fluxes must have been very high to effect the observed Si removal or redistribution. This effect is only enhanced if CO_2 is also involved, as it also reduces quartz solubility (Fig. 2).

5. Implications

- Quartz solubility declines exponentially as $CaCl_2$ is added to H2O at all P and T investigated.
- The decreases in solubility imply that there is no complex formation between SiO2 and the salt. This contrasts with H_2O-NaCl, where complexing appears to cause solubility enhancement. Instead, where data exist for comparison, silica concentration is nearly the same as in CO_2-H_2O at the same H_2O activity, signaling negligible silica-Ca interaction. This holds at nearly all P-T conditions investigated, with the possible exception of the dilute solutions at 0.6 GPa and 800 °C.

- The monomer-dimer model for silica speciation leads to evidence for P-T dependent dissociation of $CaCl_2$. Our model implies substantial dissociation of $CaCl_2$ at low T and high P. Transition to undissociated $CaCl_2$ takes place over a relatively narrow temperature interval at each pressure nearly independently of $CaCl_2$ concentration at a given P and T. This feature could exert important influence on solubilities and stabilities of mineral assemblages in the presence of $CaCl_2$-bearing fluids, by virtue of the associated large changes of H_2O activity.
- Important avenues for further investigation include solubility studies of quartz and major rock-forming minerals including feldspars and magnesian silicates in mixed solutions of Ca, Na and K chlorides and carbonates, at P-T conditions spanning ranges covering the middle crust to upper mantle.

Acknowledgments

Our experimental program investigating the role of salts in fluids, melts, and their interactions with minerals, has been inspired in part by contributions and intellectual leadership of Jim Webster. We thank J Blundy, L Aranovich and N Akinfiev for helpful reviews. This work was supported by National Science Foundation grants EAR 1732256 and 2124650 to CEM.

References

Akinfiev, N.N., and Diamond, L.W. (2009) A simple predictive model of quartz solubility in water-salt-CO_2 systems at temperatures up to 1000 °C and pressures up to 1000 MPa. Geochimica et Cosmochimica Acta, 73, 1597-1608.

Aranovich, L., Akinfiev, N.N., and Golunova, M. (2020) Quartz solubility in sodium carbonate solutions at high pressure and temperature. Chemical Geology, 550, 119699.

Aranovich, L.Y., and Newton, R. (1996) H_2O activity in concentrated NaCl solutions at high pressures and temperatures measured by the brucite-periclase equilibrium. Contributions to Mineralogy and Petrology, 125, 200-212.

Aranovich, L.Y., and Newton, R. (1996) (1997) H_2O activity in concentrated KCl and KCl-NaCl solutions at high temperatures and pressures measured by the brucite-periclase equilibrium. Contributions to Mineralogy and Petrology, 127, 261-271.

Brooks, H.L., and Steele-MacInnis, M. (2019) A model for the solubility of minerals in saline aqueous fluids in the crust and upper mantle. American Journal of Science, 319, 754-787.

Brovarone, A.V., and Beyssac, O. (2014) Lawsonite metasomatism: A new route for water to the deep Earth. Earth and Planetary Science Letters, 393, 275-284.

Carten, R.B. (1986) Sodium-calcium metasomatism; chemical, temporal, and spatial relationships at the Yerington, Nevada, porphyry copper deposit. Economic Geology, 81, 1495-1519.

Dahlgren, S., Bogoch, R., Magaritz, M., and Michard, A. (1993) Hydrothermal dolomite marbles associated with charnockitic magmatism in the Proterozoic Bamble Shear Belt, south Norway. Contributions to Mineralogy and Petrology, 113, 394-409.

De Jong, G., and Williams, P. (1995) Giant metasomatic system formed during exhumation of mid-crustal Proterozoic rocks in the vicinity of the Cloncurry Fault, northwest Queensland. Australian Journal of Earth Sciences, 42, 281-290.

Dolejš, D., and Manning, C.E. (2010) Thermodynamic model for mineral solubility in aqueous fluids: theory, calibration and application to model fluid-flow systems. Geofluids, 10, 20-40.

Edwards, A., and Baker, G. (1953) Scapolitization in the Cloncurry District of north-western Queensland. Journal of the Geological Society of Australia, 1, 1-33.

Eglinger, A., Tarantola, A., Durand, C., Ferraina, C., Vanderhaeghe, O., André-Mayer, A.-S., Paquette, J.-L., and Deloule, E. (2014) Uranium mobilization by fluids associated with Ca–Na metasomatism: A P–T–t record of fluid–rock interactions during Pan-African metamorphism (Western Zambian Copperbelt). Chemical Geology, 386, 218-237.

Evans, K. (2007) Quartz solubility in salt-bearing solutions at pressures to 1 GPa and temperatures to 900 ° C. Geofluids, 7, 451-467.

Fournier, R.O. (1983) A method of calculating quartz solubilities in aqueous sodium chloride solutions. Geochimica et Cosmochimica Acta 47: 579-586.

Harper, G.D. (1995) Pumpellyosite and prehnitite associated with epidosite in the Josephine ophiolite—Ca metasomatism during upwelling of hydrothermal fluids at a spreading axis. Geological Society of America Special Papers, 296, 101-122.

Holland, T.J.B. and Powell, R. (1991) A compensated-Redlich-Kwong (CORK) equation for volumes and fugacities of CO_2 and H_2O in the range 1 bar to 50 kbar and 100-1600 °C. Contributions to Mineralogy and Petrology, 109, 265-273

Holness, M.B. (1992) Equilibrium dihedral angles in the system quartz-CO_2-H_2O-NaCl at 800° C and 1–15 kbar: the effects of pressure and fluid composition on the permeability of quartzites. Earth and Planetary Science Letters, 114, 171-184.

Huang, F., and Sverjensky, D.A. (2019) Extended Deep Earth Water Model for predicting major element mantle metasomatism. Geochimica et Cosmochimica Acta, 254, 192-230.

Hunt JD, Manning CE (2012) A thermodynamic model for the system SiO_2-H_2O near the upper critical end point based on quartz solubility experiments at 500-1100 °C and 5-20 kbar. Geochimica et Cosmochimica Acta, 86, 196-213.

Ivanov, M.V., and Bushmin, S.A. (2019) Equation of state of the H_2O–CO_2–$CaCl_2$ fluid system and properties of fluid phases at P-T parameters of the middle and lower crust. Petrology, 27, 395-406.

Izraeli, E.S., Harris, J.W. and Navon, O. (2001) Brine inclusions in diamonds: a new upper mantle fluid. Earth and Planetary Science Letters, 187, 323-332.

Johannes, W. (1973) A simplified piston-cylinder apparatus of high precision. Neues Jahrbuch für Mineralogisch Monatlich, 7, 331-351.

Johannes, W., Bell, P., Mao, H., Boettcher, A., Chipman, D., Hays, J., Newton, R., and Seifert, F. (1971) An interlaboratory comparison of piston-cylinder pressure calibration using the albite-breakdown reaction. Contributions to Mineralogy and Petrology, 32, 24-38.

Kendrick, M.A., Baker, T., Fu, B., Phillips, D., and Williams, P. (2008) Noble gas and halogen constraints on regionally extensive mid-crustal Na–Ca metasomatism, the Proterozoic Eastern Mount Isa Block, Australia. Precambrian Research, 163, 131-150.

Manning, C.E. (1994) The solubility of quartz in H_2O in the lower crust and upper mantle. Geochimica et Cosmochimica Acta, 58, 4831-4839.

Mark, G. (1998) Albitite formation by selective pervasive sodic alteration of tonalite plutons in the Cloncurry district, Queensland. Australian Journal of Earth Sciences, 45, 765-774.

Mark, G., Oliver, N., and Carew, M.J. (2006) Insights into the genesis and diversity of epigenetic Cu–Au mineralisation in the Cloncurry district, Mt Isa Inlier, northwest Queensland. Australian Journal of Earth Sciences, 53, 109-124.

Mavrogenes, J., and Blundy, J. (2017) Crustal sequestration of magmatic sulfur dioxide. Geology, 45, 211-214.

Mirwald, P.W., Getting, I.C., and Kennedy, G.C. (1975) Low-friction cell for piston-cylinder high-pressure apparatus. Journal of Geophysical Research, 80, 1519-1525.

Moecher, D., Essene, E., and Valley, J. (1992) Stable isotopic and petrological constraints on scapolitization of the Whitestone meta-anorthosite, Grenville Province, Ontario. Journal of Metamorphic Geology, 10, 745-762.

Newton, R.C., and Manning, C.E. (2000) Quartz solubility in H_2O-NaCl and H_2O-CO_2 solutions at deep crust-upper mantle pressures and temperatures: 2–15 kbar and 500–900 ºC. Geochimica et Cosmochimica Acta, 64, 2993-3005.

Newton, R.C., and Manning, C.E. (2002) Solubility of enstatite+ forsterite in H_2O at deep crust/upper mantle conditions: 4 to 15 kbar and 700 to 900 °C. Geochimica et Cosmochimica Acta, 66, 4165-4176.

Newton, R.C., and Manning, C.E. (2003) Activity coefficient and polymerization of aqueous silica at 800 °C, 12 kbar, from solubility measurements on SiO_2-buffering mineral assemblages. Contributions to Mineralogy and Petrology, 146, 135-143

Newton, R.C., and Manning, C.E. (2006) Solubilities of corundum, wollastonite and quartz in H_2O–NaCl solutions at 800 C and 10 kbar: interaction of simple minerals with brines at high pressure and temperature. Geochimica et Cosmochimica Acta, 70, 5571-5582.

Newton, R.C., and Manning, C.E. (2008) Thermodynamics of SiO_2–H_2O fluid near the upper critical end point from quartz solubility measurements at 10 kbar. Earth and Planetary Science Letters, 274, 241-249.

Newton, R.C., and Manning, C.E. (2009) Hydration state and activity of aqueous silica in H_2O-CO_2 fluids at high pressure and temperature. American Mineralogist, 94, 1287-1290.

Newton, R.C., and Manning, C.E. (2010) Role of saline fluids in deep-crustal and upper-mantle metasomatism: insights from experimental studies. Geofluids, 10, 58-72.

Newton, R.C., and Manning, C.E. (2016) Evidence for SiO_2-NaCl complexing in H_2O-NaCl solutions at high pressure and temperature. Geofluids, 16, 342-348.

Novgorodov, P. (1975) Solubility of quartz in an H_2O-CO_2 mixture at 700 degrees C and pressures of 3 and 5 kbars. Geokhimiya, 10, 1484-1489.

Novgorodov, P. (1977) On the solubility of quartz in H_2O+CO_2 and H_2O+NaCl at 700 °C and 1.5 kb pressure. Geochemistry International, 14, 191-193.

Oliver, N.H., Rawling, T.J., Cartwright, I., and Pearson, P.J. (1994) High-temperature fluid-rock interaction and scapolitization in an extension-related hydrothermal system, Mary Kathleen, Australia. Journal of Petrology, 35, 1455-1491.

Python, M., Yoshikawa, M., Shibata, T., and Arai, S. (2011). Diopsidites and rodingites: Serpentinisation and Ca-Metasomatism in the Oman ophiolite mantle. In R.K. Srivastava, Ed., Dyke Swarms: Keys for Geodynamic Interpretation, p. 401-435. Springer, Berlin.

Quist, A.S., and Marshall, W.L. (1966) Electrical conductances of aqueous solutions at high temperatures and pressures. III. The conductances of potassium bisulfate solutions from 0 to 700 ° and at pressures to 4000 bars. The Journal of Physical Chemistry, 70, 3714-3725.

Schulze, D.J. (1995) Low-Ca garnet harzburgites from Kimberley, South Africa: Abundance and bearing on the structure and evolution of the lithosphere. Journal of Geophysical Research: Solid Earth, 100, 12513-12526.

Setchenow, M. (1892) Action de l'acide carbonique sur les solutions des sels a acides forts. Annales de Chimie et de Physique, 25, 226-270.

Shmulovich, K., Yardley, B., and Graham, C. (2006) Solubility of quartz in crustal fluids: experiments and general equations for salt solutions and H_2O–CO_2 mixtures at 400–800 °C and 0.1–0.9 GPa. Geofluids, 6(2), 154-167.

Sverjensky, D.A., Harrison, B., and Azzolini, D. (2014) Water in the deep Earth: The dielectric constant and the solubilities of quartz and corundum to 60 kb and 1200 °C. Geochimica et Cosmochimica Acta, 129, 125-145.

Touret, J.L.R., and Nijland, T.G. (2013). Prograde, peak and retrograde metamorphic fluids and associated metasomatism in upper amphibolite to granulite facies transition zones. In Harlov, D.E., and Austerheim, H., Eds., Metasomatism and the Chemical Transformation of Rock, p. 415-469. Springer, Berlin.

Walther, J.V., and Orville, P.M. (1983) The extraction-quench technique for determination of the thermodynamic properties of solute complexes; application to quartz solubility in fluid mixtures. American Mineralogist, 68, 731-741.

Wickham, S., Janardhan, A., and Stern, R. (1994) Regional carbonate alteration of the crust by mantle-derived magmatic fluids, Tamil Nadu, South India. The Journal of Geology, 102, 379-398.

Xie, Z., and Walther, J.V. (1993) Quartz solubilities in NaCl solutions with and without wollastonite at elevated temperatures and pressures. Geochimica et Cosmochimica Acta, 57, 1947-1955.

Zhang, Y.-G., and Frantz, J.D. (2000) Enstatite-forsterite-water equilibria at elevated temperatures and pressures. American Mineralogist, 85, 918-925.

Zotov, N., and Keppler, H. (2000) In-situ Raman spectra of dissolved silica species in aqueous fluids to 900 °C and 14 kbar. American Mineralogist, 85, 600-604

Zotov, N., and Keppler, H. (2002) Silica speciation in aqueous fluids at high pressures and high temperatures. Chemical Geology, 184, 71-82.

This is the peer-reviewed, final accepted version for American Mineralogist, published by the Mineralogical Society of America.
The published version is subject to change. Cite as Authors (Year) Title. American Mineralogist, in press.
DOI: https://doi.org/10.2138/am-2022-8387. http://www.minsocam.org/

Table 1. Experimental results

Run	P	T	t	H_2O	$CaCl_2$	Δwt_{quartz}	X_{CaCl2}	m_{SiO2}	Notes
	GPa	°C	hr	mg	mg	mg		mol/kg H_2O	
QzC-47	0.6	600	22.0	19.662	0.000	0.366(1)	0.000	0.310(1)	
QzC-52	0.6	600	18.0	28.311	20.017	0.254(1)	0.103	0.149(1)	
QzC-36	0.6	600	22.0	14.976	22.512	0.063(1)	0.196	0.070(1)	
QzC-39	0.6	700	22.0	15.767	0.000	0.488(2)	0.000	0.515(2)	
QzC-76	0.6	700	23.0	20.926	3.287	0.608(1)	0.025	0.483(1)	
QzC-46	0.6	700	20.0	26.690	8.497	0.687(1)	0.049	0.429(1)	
QzC-54	0.6	700	22.0	20.457	14.021	0.398(1)	0.100	0.324(1)	
QzC-57	0.6	700	24.5	14.174	21.201	0.129(2)	0.195	0.152(2)	
QzC-45	0.6	700	28.5	10.792	28.596	0.051(2)	0.300	0.078(3)	
QzC-35	0.6	800	4.0	24.916	0.000	1.321(1)	0.000	0.883(1)	
QzC-40	0.6	800	22.0	24.841	0.000	1.353(2)	0.000	0.906(1)	
QzC-74	0.6	800	22.0	15.580	2.511	0.864(2)	0.025	0.923(2)	
QzC-56	0.6	800	14.5	37.115	11.994	1.871(2)	0.050	0.839(1)	max (2)
QzC-37	0.6	800	21.0	20.110	14.170	0.689(3)	0.103	0.570(1)	max (1)
QzC-41	0.6	800	20.5	23.662	36.169	0.484(1)	0.199	0.340(1)	
QzC-43	0.6	800	22.5	10.639	27.371	0.122(2)	0.295	0.191(3)	
QzC-108	1.0	600	69.0	10.692	0.972	0.200(1)	0.015	0.312(1)	
QzC-107	1.0	600	69.0	7.968	1.962	0.120(1)	0.038	0.252(3)	
QzC-16	1.0	600	23.0	40.060	29.726	0.375(1)	0.107	0.156(1)	
QzC-19	1.0	600	63.0	16.365	24.861	0.070(1)	0.198	0.071(1)	
QzC-28	1.0	600	1.5	21.959	47.450	0.060(1)	0.260	0.046(1)	TS
QzC-95	1.0	600	4.5	7.218	15.464	0.018(2)	0.258	0.042(2)	TS
QzC-97	1.0	600	9.0	17.112	37.769	0.039(1)	0.264	0.038(1)	TS
QzC-96	1.0	600	18.0	9.592	20.401	0.027(1)	0.257	0.047(1)	TS
QzH2O-1	1.0	700	4.0	23.951	0.000	1.040(1)	0.000	0.722(1)	
QzH2O-2	1.0	700	4.0	15.030	0.000	0.654(1)	0.000	0.724(1)	
QzC-3	1.0	700	22.5	24.598	2.794	0.950(1)	0.018	0.643(1)	
QzC-110	1.0	700	23.5	11.956	3.022	0.399(1)	0.039	0.556(1)	
QzC-9	1.0	700	47.0	17.366	6.903	0.438(1)	0.061	0.420(1)	
QzC-4	1.0	700	20.5	24.667	15.864	0.493(1)	0.095	0.332(1)	
QzC-5	1.0	700	23.0	22.386	32.609	0.238(2)	0.191	0.177(1)	
QzC-6	1.0	700	22.5	15.063	42.589	0.079(1)	0.315	0.088(1)	
QzC-91	1.0	700	22.0	8.882	44.128	0.019(1)	0.446	0.036(1)	
QzC-115	1.0	700	3.0	5.122	31.410	0.014(1)	0.499	0.046(3)	
QzC-112	1.0	800	3.8	9.271	0.000	0.759(1)	0.000	1.363(1)	
QzC-104	1.0	800	4.0	10.411	0.000	0.805(1)	0.000	1.287(1)	
QzC-101	1.0	800	4.0	23.156	0.767	1.863(1)	0.005	1.339(1)	
QzC-102	1.0	800	4.0	11.645	1.063	0.891(2)	0.015	1.273(2)	
QzC-98	1.0	800	4.0	18.575	3.158	1.256(1)	0.027	1.125(1)	
QzC-99	1.0	800	4.0	15.781	4.095	1.026(2)	0.040	1.083(2)	
QzC-10	1.0	800	21.0	29.454	11.978	1.624(2)	0.062	0.918(1)	max (1)
QzC-92	1.0	800	4.0	29.403	19.893	1.118(1)	0.099	0.633(1)	
QzC-15	1.0	800	23.0	29.393	25.065	1.077(2)	0.122	0.610(1)	max (1)
QzC-14	1.0	800	20.0	22.939	36.542	0.453(2)	0.205	0.329(1)	
QzC-12	1.0	800	25.0	14.634	30.060	0.217(2)	0.250	0.246(3)	
QzC-27	1.0	800	2.0	15.301	44.206	0.172(2)	0.319	0.187(2)	
QzC-87	1.0	800	22.0	12.567	49.656	0.092(1)	0.391	0.122(1)	
QzC-89	1.0	800	17.0	10.143	59.182	0.042(1)	0.486	0.068(1)	
QzC-105	1.0	900	4.5	14.877	0.000	2.210(1)	0.000	2.473(1)	
QzC-103	1.0	900	4.5	12.869	1.209	1.655(1)	0.015	2.140(1)	
QzC-106	1.0	900	4.5	17.658	4.436	1.896(1)	0.039	1.787(1)	
QzC-25	1.0	900	1.5	44.871	17.823	4.662(2)	0.061	1.729(1)	max (1)
QzC-100	1.0	900	4.5	14.673	7.925	1.119(1)	0.081	1.269(1)	

This is the peer-reviewed, final accepted version for American Mineralogist, published by the Mineralogical Society of America.
The published version is subject to change. Cite as Authors (Year) Title. American Mineralogist, in press.
DOI: https://doi.org/10.2138/am-2022-8387. http://www.minsocam.org/

QzC-17	1.0	900	2.5	30.023	27.301	1.685(1)	0.129	0.934(1)	
QzC-20	1.0	900	26.0	13.645	27.402	0.379(1)	0.246	0.463(1)	
QzC-24	1.0	900	19.5	17.136	51.042	0.286(3)	0.326	0.278(3)	max (1)
QzC-90	1.0	900	3.0	13.681	55.937	0.194(2)	0.399	0.237(3)	max (1)
QzC-88	1.0	900	4.0	11.099	64.505	0.116(1)	0.485	0.174(2)	
QzC-49	1.4	600	25.0	19.497	0.000	0.522(1)	0.000	0.445(1)	
QzC-73	1.4	600	72.0	23.139	7.469	0.370(1)	0.050	0.266(1)	
QzC-65	1.4	600	20.0	47.055	31.966	0.468(1)	0.099	0.165(1)	
QzC-66	1.4	600	71.0	14.757	22.980	0.071(2)	0.202	0.080(2)	
QzC-51	1.4	600	17.5	19.613	52.239	0.053(1)	0.302	0.045(1)	
QzC-71	1.4	700	51.0	37.575	13.347	1.345(1)	0.055	0.596(1)	
QzC-67	1.4	700	24.0	40.148	27.538	0.843(3)	0.100	0.349(1)	max (1)
QzC-70	1.4	700	21.0	23.985	36.910	0.252(1)	0.200	0.175(1)	
QzC-60	1.4	700	22.0	12.329	34.514	0.065(2)	0.312	0.088(1)	
QzC-72	1.4	800	18.0	23.293	7.612	1.550(1)	0.050	1.107(1)	
QzC-68	1.4	800	20.0	19.550	13.261	0.764(3)	0.099	0.650(2)	max (1)
QzC-63	1.4	800	23.5	21.050	31.598	0.423(2)	0.196	0.334(1)	
QzC-59	1.4	800	21.5	13.375	37.237	0.154(1)	0.311	0.191(1)	
QzC-75	1.4	900	23.0	25.619	8.202	3.018	0.049	1.960(1)	
QzC-69	1.4	900	20.0	18.727	14.564	1.277	0.112	1.135(3)	
QzC-83	1.4	900	5.0	15.717	23.790	0.589	0.197	0.623(1)	
QzC-61	1.4	900	22.5	23.771	37.673	0.977	0.205	0.684(14)	max (1)
QzC-84	1.4	900	5.0	17.435	37.254	0.445	0.258	0.425(1)	
QzC-58	1.4	900	21.5	12.464	33.039	0.287	0.301	0.383(4)	max (1)
QzC-85	1.4	900	4.5	16.141	45.314	0.359	0.313	0.370(2)	

Explanation: Quartz solubility results reported as weight change in single quartz crystals (Δwt_{quartz}). Parenthetical entries in Δwt_{quartz} and SiO_2 molality are 1σ uncertainty in last digit(s) based on propagated weighing errors; propagated errors in fluid compositions (X_{CaCl2}) are too low to be reported at this level. Entries in notes column: TS, time series used to determine minimum run times; max (1), maximum solubility because crystal broke; max (2), maximum solubility because run products include several minute vapor transport crystals.

Table 2. Values of α from experiments and models

P (GPa)	T (°C)	Regression of experimental data	Eq. (13)
0.6	600	0.781	0.563
0.6	700	0.139	0.043
0.6	800	-0.162	0.003
1.0	600	1.232	1.183
1.0	700	0.585	0.449
1.0	800	0.173	0.116
1.0	900	0.258	0.027
1.4	600	1.554	1.393
1.4	700	0.603	1.000
1.4	800	0.395	0.617
1.4	900	0.487	0.339

Figure captions

Figure 1. Results of experiments on quartz solubility in H_2O-$CaCl_2$ solutions at 0.6 GPa (Fig 1a), 1.0 GPa (Fig. 1b) and 1.4 GPa (Fig. 1c). Data are from Table 1; 2σ errors are smaller than symbol size. Symbols indicate temperature of experiment: circles, 600 °C; squares, 700 °C; diamonds, 800 °C; triangles, 900 °C. Filled symbols indicate solubility measurements from crystals that were unfractured, whereas unfilled symbols indicate a maximum solubility because the crystal broke or new crystals grew in the experiment. Grey symbols indicate pure-H_2O solubility from Hunt and Manning (2012). The linear trends in the log-linear plots show that solubility of quartz decreases exponentially with increasing mole fraction of $CaCl_2$ in solution. Figure 2d shows data at each temperature. Filled symbols, 0.6 GPa; open symbols, 1.0 GPa; grey symbols, 1.4 GPa. At each temperature, data at $X_{CaCl2} < 0.1$ vary with pressure, but at >0.1 are independent of pressure. This is interpreted to indicate a transition to fused salt behavior in the solvent (see text).

Figure 2. Quartz solubility at 800 °C, 1 GPa. (A) Solubility variation with H_2O mole fraction in H_2O-$CaCl_2$ (circles, this study), H_2O-CO_2 (squares, Newton and Manning, 2000, 2009), and H_2O-NaCl (diamonds, Newton and Manning (2000). (B) Solubility in H_2O-$CaCl_2$ along with representative values of $\alpha = 0$, 1 and 2 (dotted lines). A best-fit value of 0.17 (solid line) implies that $CaCl_2$ is nearly fully associated at this P and T. The model of Ivanov and Bushmin (2019) gives $\alpha = 1.51$ (dash-dot line), which does not reproduce the data. (C) As in (A), except the x axis is H_2O activity. The similar dependence of solubility on H_2O activity in the H_2O-$CaCl_2$ and H_2O-CO_2 systems suggests negligible calcium silicate complexing, in contrast to the H_2O-NaCl system.

Figure 3. Quartz solubility in H_2O-$CaCl_2$. As in Fig. 1, except solid lines are calculated using α derived from Eqs. 13-15.

Figure 4. Results of Shmulovich et al. (2006) on quartz solubility in H_2O-$CaCl_2$ at 0.5 GPa (A) and 0.9 GPa (B). Dashed lines show solubility based on their Setchénow model (Eq. 16); solid lines calculated using α (Eqs. 13-15).

Figure 5. Variation in α with H_2O density (Eqs. 13-15). Solid lines show isobars, dashed lines show isotherms. Model results suggest that at lower crustal and upper mantle pressures, decreasing temperature results in significant $CaCl_2$ ionization.

Figure 5. Predicted variation in H_2O activity with H_2O mole fraction, based on Eqs. 10 and 13-15. (A) 700 °C, 1 GPa, with values of α = 0, 1, and 2 for reference, along with results from this study and Ivanov and Bushmin (2019). Values of α in the latter work are nearly constant at $\alpha \sim$ 0.15 over all P and T of this study. For clarity, they are omitted from (B), (C) and (D) which show calculated *a-X* relations based on the present model. Our model predicts significant variation in the ionization state of CaCl2 at these conditions, such that aH2O depends strongly on P and T at any X_{CaCl2}.

This is the peer-reviewed, final accepted version for American Mineralogist, published by the Mineralogical Society of America.
The published version is subject to change. Cite as Authors (Year) Title. American Mineralogist, in press.
DOI: https://doi.org/10.2138/am-2022-8387. http://www.minsocam.org/

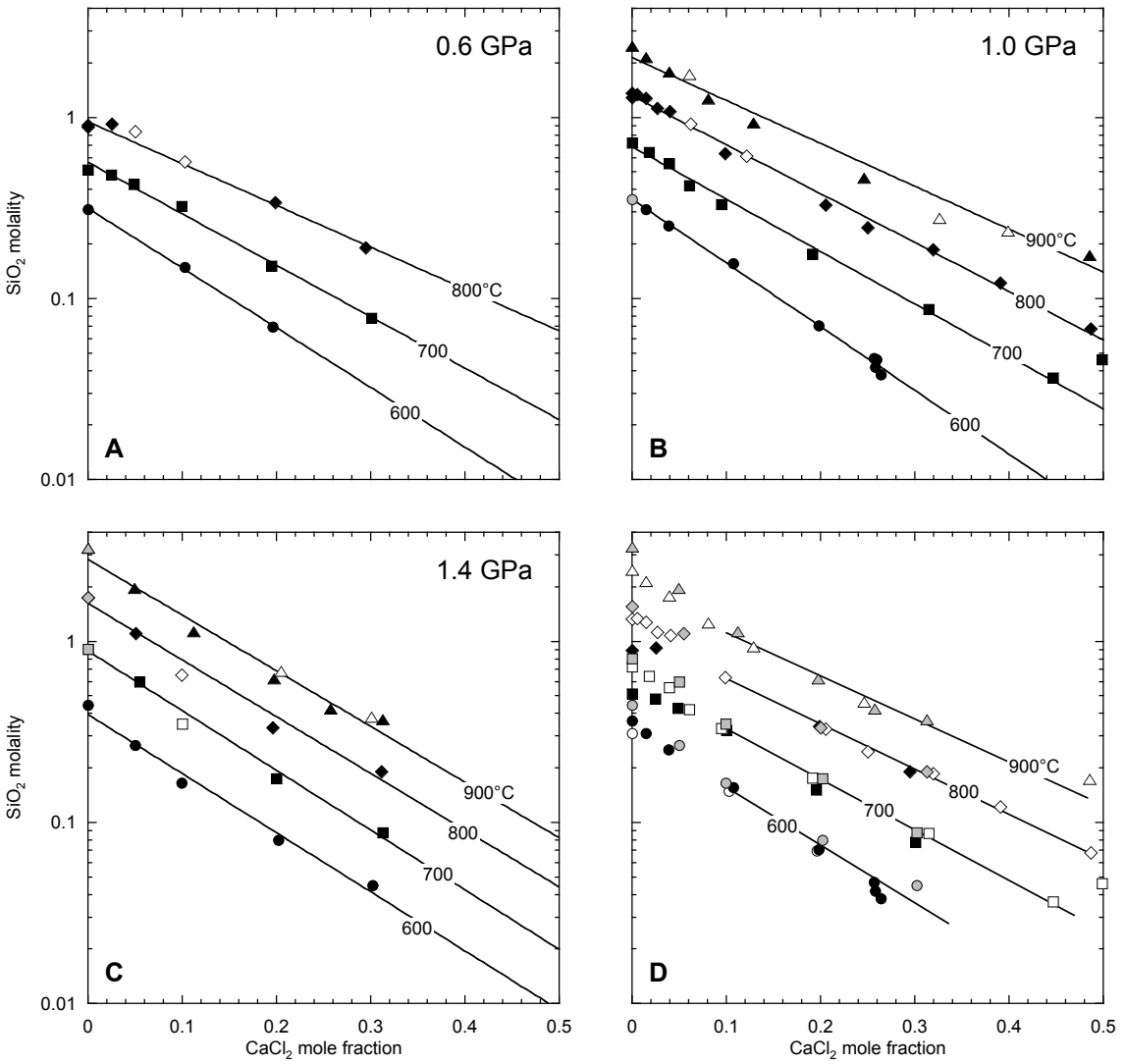

Figure 1

This is the peer-reviewed, final accepted version for American Mineralogist, published by the Mineralogical Society of America.
The published version is subject to change. Cite as Authors (Year) Title. American Mineralogist, in press.
DOI: https://doi.org/10.2138/am-2022-8387. http://www.minsocam.org/

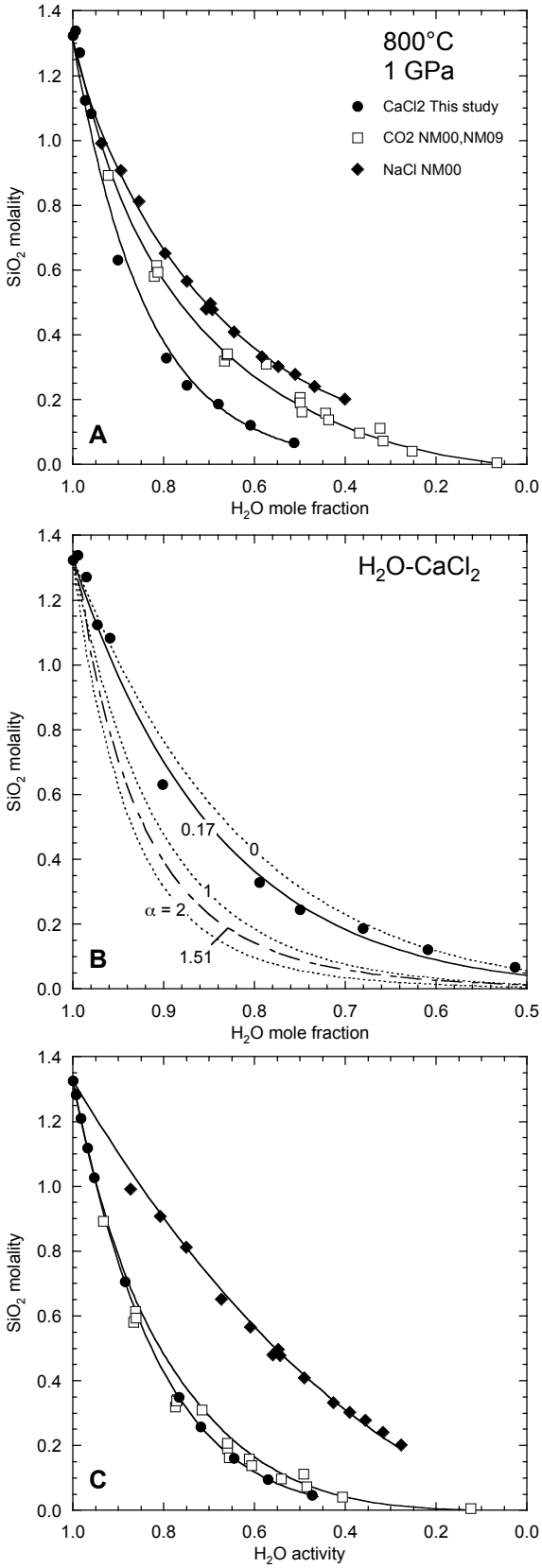

Figure 2

This is the peer-reviewed, final accepted version for American Mineralogist, published by the Mineralogical Society of America.
The published version is subject to change. Cite as Authors (Year) Title. American Mineralogist, in press.
DOI: https://doi.org/10.2138/am-2022-8387. http://www.minsocam.org/

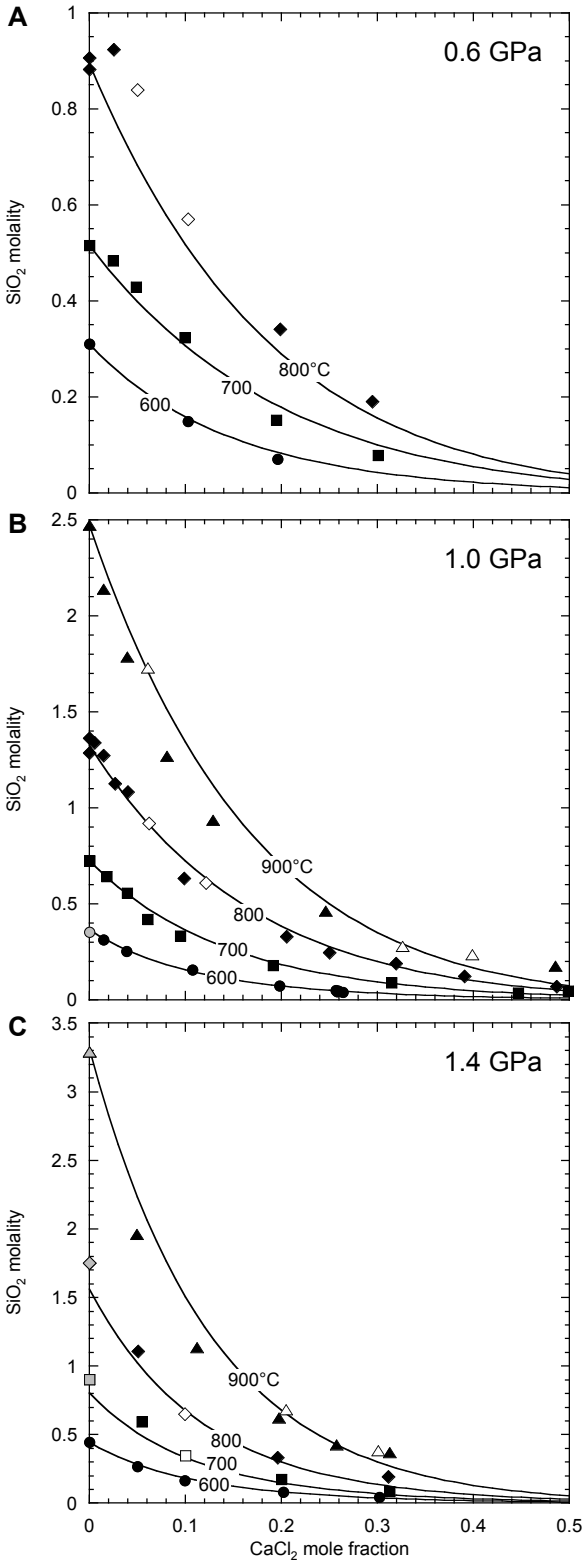

Figure 3

This is the peer-reviewed, final accepted version for American Mineralogist, published by the Mineralogical Society of America.
The published version is subject to change. Cite as Authors (Year) Title. American Mineralogist, in press.
DOI: https://doi.org/10.2138/am-2022-8387. http://www.minsocam.org/

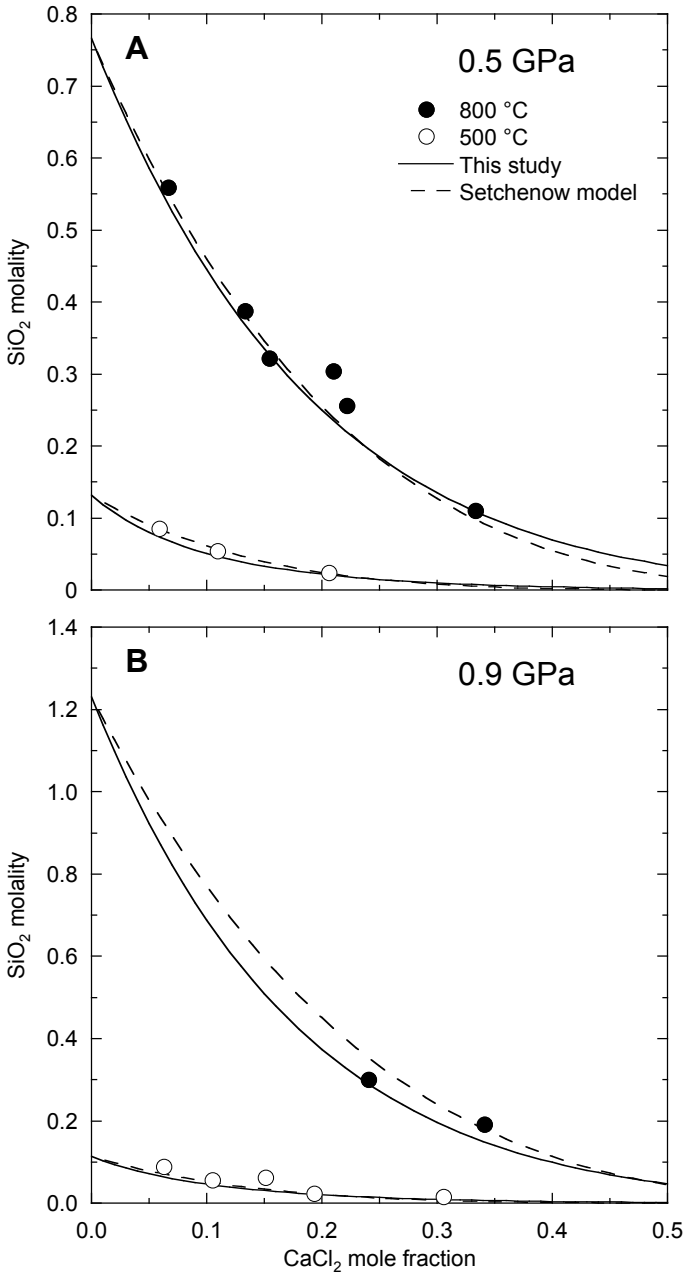

Figure 4

This is the peer-reviewed, final accepted version for American Mineralogist, published by the Mineralogical Society of America.
The published version is subject to change. Cite as Authors (Year) Title. American Mineralogist, in press.
DOI: https://doi.org/10.2138/am-2022-8387. http://www.minsocam.org/

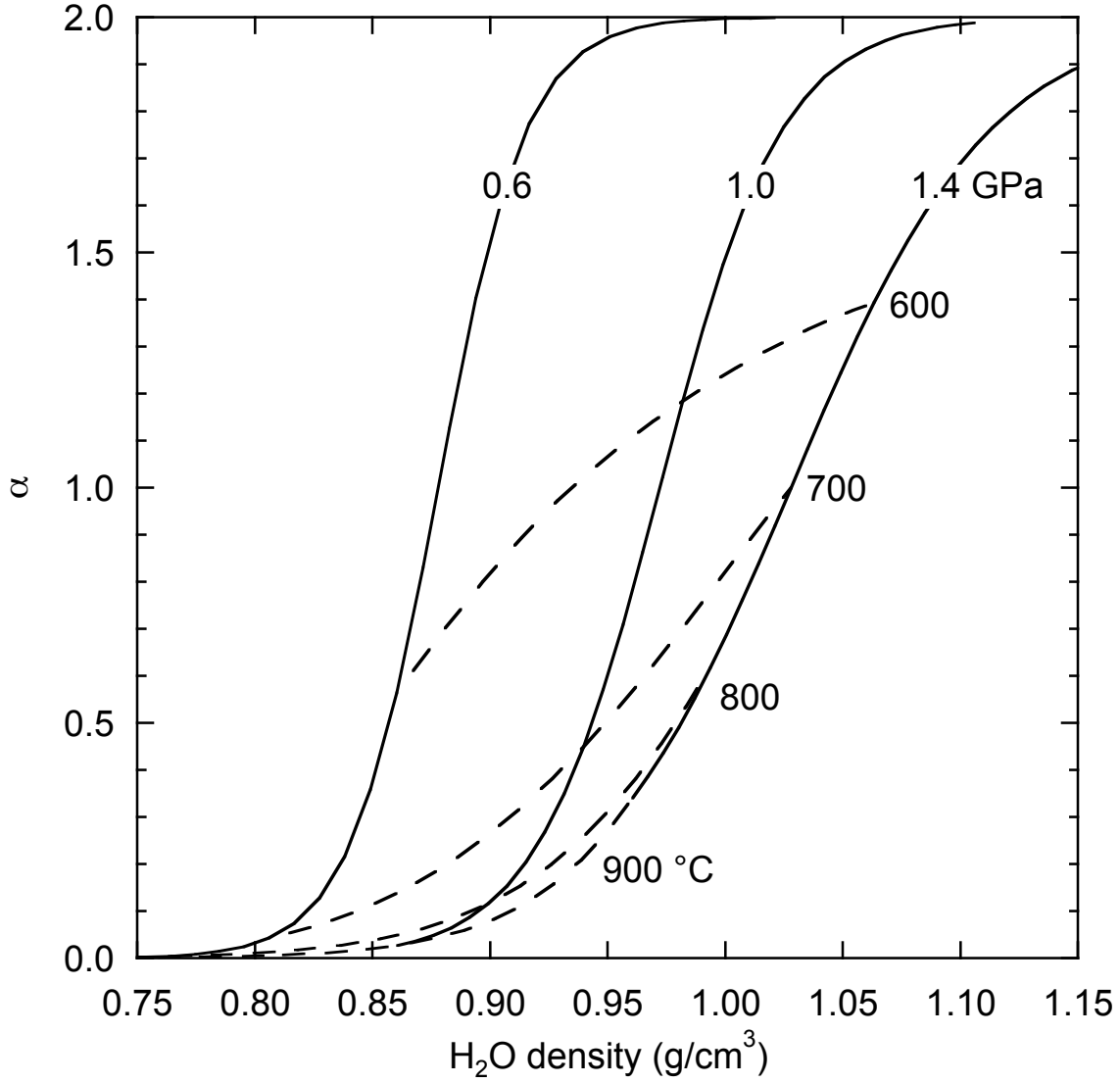

Figure 5

This is the peer-reviewed, final accepted version for American Mineralogist, published by the Mineralogical Society of America.
The published version is subject to change. Cite as Authors (Year) Title. American Mineralogist, in press.
DOI: https://doi.org/10.2138/am-2022-8387. http://www.minsocam.org/

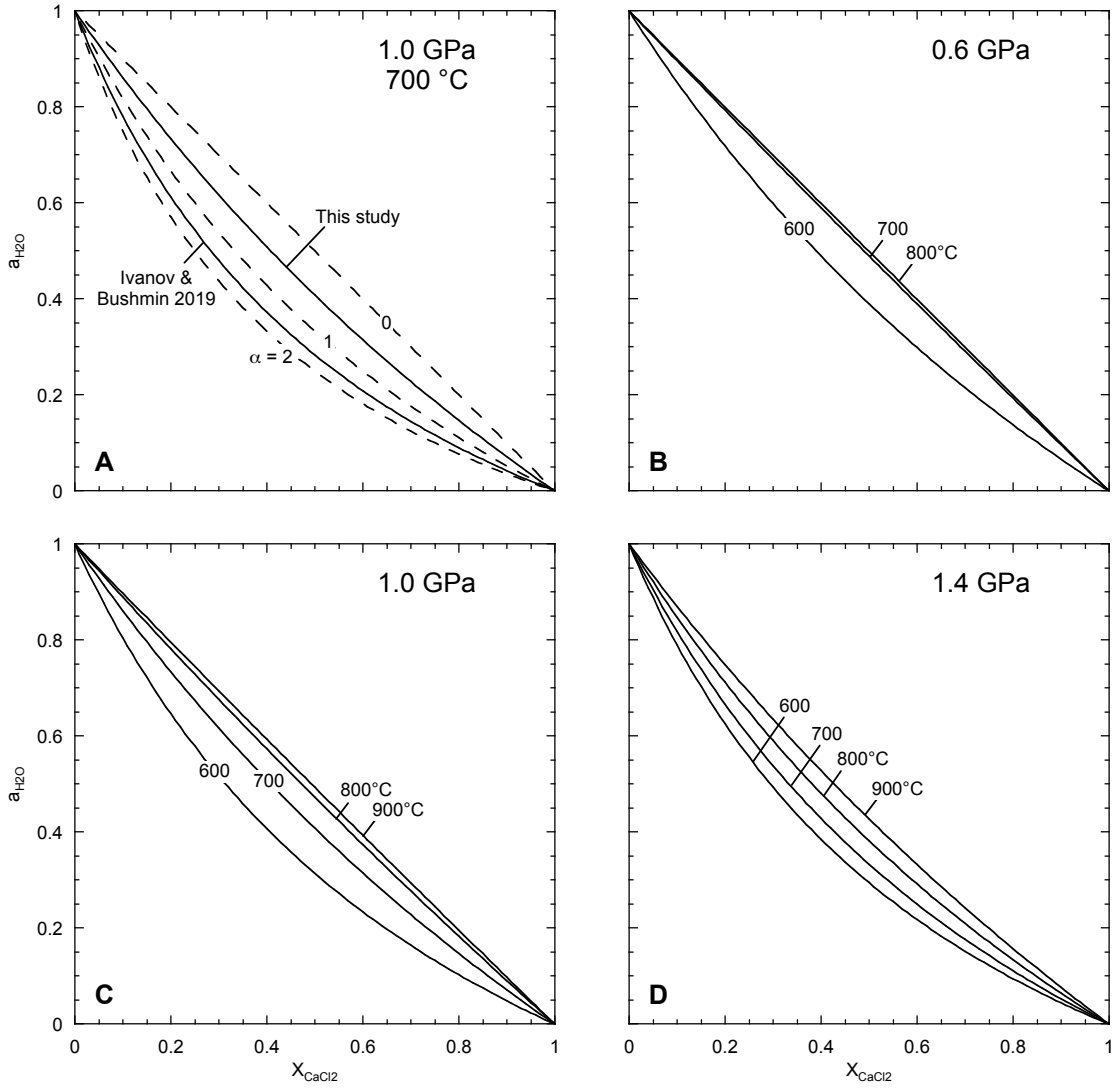

Figure 6